Particle Image Velocimetry of Collapsing Toroidal Droplets

A Thesis
Presented to
The Academic Faculty

by

Eric M. Berger

In Partial Fulfillment
of the Requirements for the Degree
Bachelors of Science

School of Physics
Georgia Institute of Technology
April 2015

Particle Image Velocimetry of Collapsing Toroidal Droplets

Approved by:

Professor Alberto Fernandez-Nieves

Professor Edwin Greco

Date Approved 4/30/15

To my parents,

Keith and Beth Berger,

for always believing in me.

PREFACE

This dissertation is the original, unpublished, joint work of the author, Eric M. Berger, and his mentors Dr. Ekapop Pairam and Professor Fernandez-Nieves.

ACKNOWLEDGEMENTS

I want to thank Alex Fragkopoulos, Dr. Ekapop Pairam, and Dr. Alberto Fernandez-Nieves for being exceptional mentors and guides while I worked on the research project outlined in this thesis. In addition, I want to thank Perry Ellis, Hung Le, John Hyatt, Michael Tennenbaum, Winnie Cheng and Carthik Nayani for being extremely supportive lab members, co-workers, and friends. Finally, I want to thank Dr. Edwin Greco for providing meaningful feedback and helpful advice throughout the thesis writing process.

ABSTRACT

The goal of this study is to explore the mechanism by which unstable toroidal droplets collapse inwardly. As such, particle image velocimetry methods will be employed in obtaining an experimental picture of the velocity field inside of unstable toroidal droplets as they collapse. The inward collapse exhibited by unstable toroidal droplets is unique to the geometry of the torus and is therefore physically interesting. There is currently not an available experimental picture of this collapse, so this study will attempt to fill that void. Ultimately the results of this study will be compared against the currently accessible theoretical pictures of collapsing toroidal droplets, leading to further refinements in the field.

TABLE OF CONTENTS

LIST OF FIGURES

CHAPTER I

INTRODUCTION

Bubbles and droplets are physical systems encountered frequently in everyday life. They makeup raindrops and clouds, and are essential for the production of many health and wellness products, ranging from ubiquitous shaving creams to complex drug delivery systems [1]. Droplets also come into play with many food products that we all know and depend upon[2]. In nature, stationary bubbles and droplets tend to have a spherical shape, a result of minimizing area [1]. As a result, when a gas or a liquid is released into an immiscible medium, it will tend towards sphere formation. However, in the presence of external forces, one can exploit the nature of immiscible fluids to generate non-spherical shapes. Plateau was the first to demonstrate this feature experimentally in his groundbreaking paper [7], where a variety of non-spherical equilibrium shapes where exhibited by water droplets subjected to sufficient spinning. These equilibrium shapes theoretically included the torus, which showed that despite inherent instability, toroidal droplets could potentially be generated in a laboratory setting. Plateau's methods were further refined in 2008, when Hill and Eaves demonstrated similar equilibrium states through magnetic levitation and rotation of water droplets [3]. Another instance of unstable toroidal droplets generated in a laboratory setting is discussed in Walters and Davidson's 1963 paper, where bursts of air were injected through a bath of water and evolved into various shapes, including the torus [9].

In addition to torus formation through the rotation or acceleration of droplets in a viscous medium, Pairam and Fernandez-Nieves showed that toroidal droplets can be generated in a very controlled manner by injecting a jet of fluid into a rotating bath of a viscous immiscible fluid [5]. Their method works because of the viscous drag exerted by the outer fluid on the injected fluid, causing the formation of a circular jet at the tip of the needle. The toroidal droplet is formed when the jet completely curves around and closes in on itself. In their study, a surfactant was added to the inner fluid in order to lower the surface tension between media, in order to allow for easier generation of tori.

When toroidal droplets are suspended in a viscous medium, they inevitably transform into stable spherical droplets through curious means. Toroidal droplets composed of thin tubes, relative to their overall diameter, tend to break apart into one or several small spherical droplets. As Pairam and Fernandez-Nieves showed, this pattern is a result of the same forces that drive the breakup of a cylindrical jet. Cylindrical jets, of course, break up in the manner of the most unstable wavelength mode that is able to grow within the cylinder[6][8]. Despite this similarity, a degree of inward shrinkage is also apparent in the torus. In toroidal droplets with relatively fat tubes and small overall diameters, an unstable wavelength is unable to grow, and inward shrinkage appears to dominate. As such, these tori collapse centrally into single spherical drops. This manner of shrinking and subsequent coalescence is unique to the geometry of the toroidal droplet, and is therefore physically interesting. Unfortunately, their paper failed to provide an experimental picture of the velocity field within these fat toroidal droplets.

Yao and Bowick proposed a theory that accurately captured the shrinking speed associated to this collapse [10]. By imposing specific boundary conditions and making use of known fluid mechanics, Yao and Bowick matched the experimentally observed shrinking speed. For fat toroidal droplets of small overall radius, their theory proposed a shrinking instability driven by a pressure differential caused by the geometry of the torus. After proposing their mathematical picture, Yao and Bowick further attempted to model a theoretical flow field for the fluid within the toroidal droplet. Though experimental flow-field data was unavailable, other aspects of his model held strongly against the available experimental data of Pairam and Fernandez-Nieves.

The intent of this paper is to experimentally reveal and analyze the velocity fields that occur within fat toroidal droplets as they collapse inwardly. In order to quantify the shrinking instability that drives this collapse, Particle Image Velocimetry techniques will be utilized in an attempt to capture the velocity fields within collapsing toroidal droplets. Eventually the data produced through this study will be compared against the theoretical predictions of Yao and Bowick, in an attempt to either confirm or dispute their projected physical model.

CHAPTER II

LITERATURE REVIEW

The study of unstable toroidal droplets has gained recent popularity in the world of soft condensed matter physics[5][10][4], and this buttressing popularity can be largely attributed to recent developments in the field. However, the key principals that drive the current study of unstable toroidal droplets lie within a well-developed realm of fluid mechanics that entered the limelight hundreds of years ago. Plateau was the first to theorize that bubbles and droplets could exhibit non-spherical equilibrium shapes in the presence of certain external forces[7]. Plateau's methods and theories have been refined and implemented over the years in such ways that toroidal droplets can be reliably generated in a laboratory setting. To date, many aspects of unstable toroidal droplets have been critically analyzed, and many theories have been proposed as to the specific mechanism that drives the collapse of these droplets. Despite these studies, no researcher has been able to effectively reveal what happens within unstable toroidal droplets as they collapse–a crucial piece of the puzzle that has the potential to completely characterize the breakup of unstable toroidal droplets.

The true origin of the study of unstable toroidal droplets can be attributed to Plateau. His groundbreaking 1873 publication entitled, "Experimental and Theoretical Statics of Liquids subject to Molecular Forces" served as an extremely comprehensive study of the forces that control the equilibrium shapes of fluid droplets. His work begins with an explanation of the geometrical constraints that drive all liquids to spherical configurations in the absence of gravity. Plateau explains that the equilibrium shape of a fluid must have equal principal curvatures at all points. Spheres are the only shapes that satisfy this condition, implying that spheres are the only possible equilibrium shape for an undisturbed fluid[7]. With this foundation developed, Plateau goes on to propose that, under certain external forces, it would be theoretically possible for fluid droplets to exhibit non-spherical shapes. Again a result of geometrical constraints, it's possible that droplets subject to sufficient rotation could exhibit a variety of non-spherical shapes, including the torus. Utilizing available

technologies, Plateau put his theory to test by rotating droplets of various immiscible fluids suspended in large baths of viscous fluids. His work revealed a plethora of non-spherical equilibrium shapes, but ultimately falls short of generating a toroidal droplet. Furthermore, his theory could not be completely tested as a result of viscous drag between the immiscible fluids, a limitation of the methods available at the time of his experiments.

It was only very recently that a more modern approach was utilized in putting Plateau's theories to test. In 2008, R.J.A. Hill published a paper that summarized an experiment in which a superconducting magnet was used to magnetically levitate droplets of water. Once levitated, the experimenters would apply a charge to the surface of the droplet, initiating a rotation as a result of the Lorentz force. This technique effectively eliminated the viscous drag encountered in Plateau's initial experiment, as the outer medium was air rather than a viscous liquid. The results of Hill's experiment showed a variety of non-spherical equilibrium shapes, including two-lobed, three-lobed, four-lobed, and five-lobed droplets[3]. This experiment again did not manage to produce a toroidal droplet, but did serve to refine the theories proposed by Plateau.

Another approach to the generation of toroidal droplets was carried out in 1968 by J.K. Walters. In this experiment, rather than subjecting fluid droplets to significant levels of external rotation, Walters imposed drag and acceleration. By injecting small pulses of air into the bottom of a tank of water, the experiment sought to determine the equilibrium shapes of the air bubbles as they traveled from the bottom of the tank to the top of the tank. The results of the experiment showed that depending on the duration of the injection and the volume of air injected, the bubbles would evolve into a series of shapes [9]. However, for sufficiently short air pulses, it was possible to generate toroidal bubbles that maintained their toroidal geometry while traveling towards the surface of the tank. Walters also went on to propose a mathematical model for the growth of these air bubbles, which incorporated a concise method for calculating the circulation of the toroidal bubbles as they moved through water. Despite providing a trivial procedure for generating toroidal droplets, the experiment and model only deal with droplets in motion or accelerating, and do not look into the instability of the droplets. Furthermore, the method used to generate toroidal droplets was not well-controlled and dealt with quickly evolving bubbles.

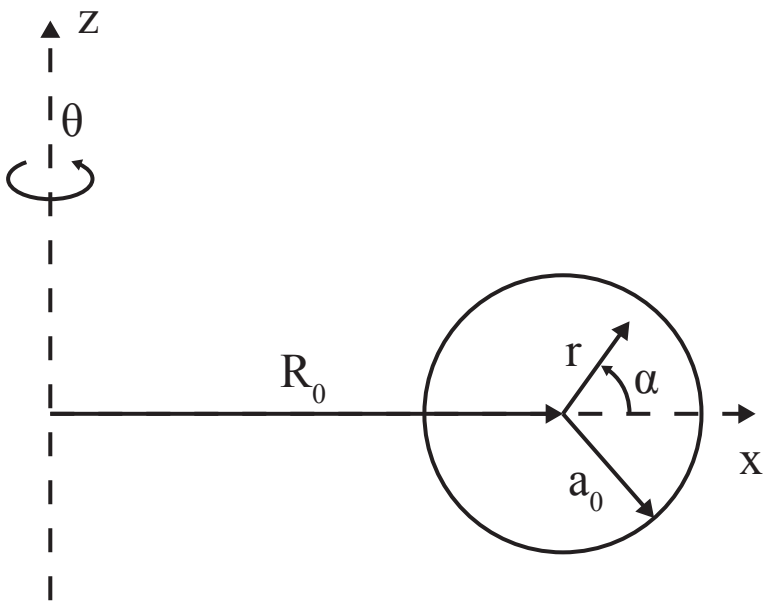

Figure 1: Geometry of the torus.

In 2009, the field encompassing the study of unstable toroidal droplets changed substantially when Pairam and Fernandez-Nieves published their paper," Generation and Stability of Toroidal Droplets in a Viscous Liquid." Their work not only provided a major investigation into the instability of toroidal droplets, but further proposed a simple method for generating well-controlled toroidal droplets in a manner such that they could be easily observed without high speed cameras. In order to generate toroidal droplets, the experimenters would inject a jet of water or glycerol through a needle into a rotating bath of viscous silicon oil. While injecting the jet and rotating the outer fluid, viscous drag would cause the jet to bend in a circular manner, eventually closing upon itself and forming a toroidal droplet. The geometry of the droplets could be varied by manipulating the location of needle and volume of inner fluid. Once the droplets were fully formed, the experimenters would remove the needle and cease the rotation of the bath, causing the unstable droplets to evolve to an equilibrium configuration [5]. Pairam and Fernandez-Nieves proposed that the breakup of the droplets resulted from a competition between the mechanism by which cylindrical jets break apart and a radial shrinkage unique to the geometry of the torus. The nature of the competition between shrinkage and break-up theoretically depended on the droplet's aspect ratio, which is defined as:

$$\xi = \frac{R_o}{a_o} \tag{1}$$

where R_o refers to the major radius of the torus and a_o refers to the minor radius, as shown in figure 1. Their theory was supported by the fact that toroidal droplets of large aspect ratio broke apart into several smaller spherical droplets, while toroidal droplets of small aspect ratio shrank inwardly until they collapsed into a single spherical droplet.

In response to the publication of Pairam and Fernandez-Nieves' paper, Mehrabian published "Capillary Breakup of a Liquid Torus," in attempt to theoretically capture the previously observed evolution of unstable toroidal droplets. While the breakup of cylindrical jets as a result of Rayleigh-Tomotika instabilities is well-understood, Mehrabian claimed that complications arise when applying this model to the toroidal droplet. The Rayleigh-Tomotika model relies on the fitting of the maximum wavelength within a cylinder, but available growth modes are affected by geometry of the toroidal droplet. The picture is further complicated by the inward shrinkage of the torus, which causes fluid flow inside the droplets. In order to provide a theoretical model, Mehrabian attempted to differentiate between the time scales that drive the two competing modes of collapse. Eventually Mehrabian showed that the manner by which unstable droplets evolve is a result of the mode that is able to grow most rapidly, a factor affected by tube thickness and diameter [4].

Another comprehensive, theoretical response to Pairam and Fernandez-Nieves' paper was carried out by Yao and Bowick, in their paper entitled The "Shrinking Instability of Toroidal Liquid Droplets" in the Stokes Flow Regime. Their paper mainly focuses on the shrinking instability that drives the inward shrinkage and eventual collapse of sufficiently fat toroidal droplets. In this theoretical model, one first minimizes the free energy of toroidal droplets that result from surface tension, then goes on to categorize a pressure differential within the toroidal droplets [10]. The model eventually manages to capture many of the shrinking qualities observed in the experiments.

Yao and Bowick's paper serves to set the stage for our research project, as an experimental attempt will be carried out to observe the velocity field of collapsing toroidal droplets. There are sufficient theoretical models of the forces that drive the breakup of unstable toroidal droplets, but no studies have experimentally confirmed or refuted any of the available theories. Through the use of Particle-Image-Velocimetry, the evolution of unstable toroidal droplets will be observed from the

inside, as tracer particles allow us to follow the flow of the inner fluid. This study will potentially either corroborate or refute Yao and Bowick's model for the proposed velocity fields.

CHAPTER III

EXPERIMENTAL METHODS

3.1 A Word on PIV

The exploration of the velocity fields within Collapsing Toroidal droplets cannot begin without a thorough explanation of Particle Image Velocimetry (PIV). Though at first glance an intimidating phrase, the precise definition of PIV is intuitive. ”Particle” refers to the fact that, in a typical PIV experiment, one selects a particulate material unique to the fluids in question, such that it will behave as though it were part of the fluid. Ideally, the chosen particles will not interfere with the overall motion of the fluid and will be of proper density such that they don't experience significant sedimentation within the timescale of the experiment. Typical particles tend to be small spheres of glass or plastic and range from nanometer radius to micrometer radius, depending on the experiment.

”Image” refers to the manner by which one observes the motion of fluids. When a proper particle is chosen, one must devise a mechanism to effectively capture images of the particles within the fluid. This is typically accomplished by shining a laser sheet through an interesting region of the fluid. As the laser sheet cuts its way through the fluid, it scatters off the particles, resulting in an effective visualization of the fluid's motion. With the fluid illuminated, some sort of imaging equipment is used to capture series of pictures of the scattered light. High-frame-rate CCD cameras are typically used for this application, though the necessary frame rate is also unique to the nature of the experiment.

”Velocimetry” refers to the method by which useful data is extrapolated from the resulting image sequences. This final piece of the PIV procedure typically involves the use of imaging software. As such, each image of the fluid is compared to the one that precedes it and the position of image features are monitored as a function of time. Ultimately, a velocity vector field results from the captured videos, which is used to gain both a qualitative and quantitative picture of the fluid motion.

3.2 Building a PIV System

The processes explored through the experiments discussed in this thesis occur at room-temperature, in liquids, in a time scale on the order of 30 seconds, and are of macroscopic size. As such, a low-cost PIV system was designed to meet the needs of the experiment at hand. Drawing on the available equipment, a 633 nm, 0.5 mW He-Ne lasers was chosen as the light source. The laser would be used in conjunction with a plano-convex cylindrical lens to create a sheet of laser light and illuminate a plane of the sample. Though mainly chosen for its immediate availability, this laser would also function well with the visible-light capturing CCD cameras intended for use in the experiment. Opaque polystyrene beads with an average size of 16.2 μm were chosen for their capability of scattering 633 nm light. In addition to the light scattering properties, having a density of 1.05$\frac{\text{g}}{\text{mL}}$, these particles would experience minimal sedimentation in the explored fluid. The preceding physical parameters of the PIV system were used in conjunction with PIV software called OpenPIV.

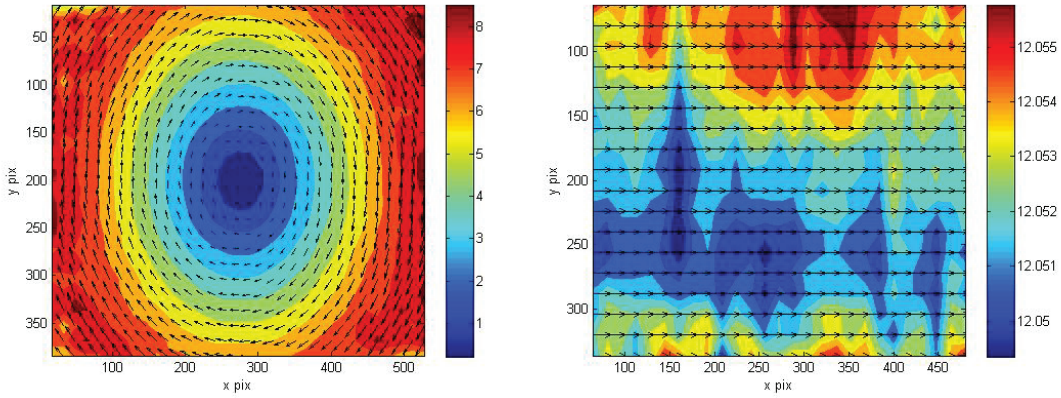

Figure 2: Rotational and translational control test results.

Before attempting any experiments, it was compulsory to ensure that the new system would operate properly and be capable of performing accurate PIV. As such, a series of tests were devised to assess the functionality of both the hardware and software components. Beginning with a test of the software, a series of control videos were generated and processed through the OpenPIV program.

The first video involved the constant horizontal translation of a pattern, with a net displacement of 12 pixels per frame. The second video involved the rotation of the same pattern, at a constant angular speed of 2 degrees per frame. The results of these tests are contained in Figure 2, with the rotational experiment on the left and the translational experiment on the right. At a qualitative level, the results of both experiments showed that OpenPIV succeeded in capturing the movement contained in the test videos. Furthermore, on a quantitative level, a good agreement was also observed. For the translational control test, OpenPIV detected a horizontal motion of 12.05 pixels per frame, which reflected an error margin of 0.41%. For the translational control test, a similar margin of 1.5% resulted from the extracted angular speed of 1.97 degrees per frame.

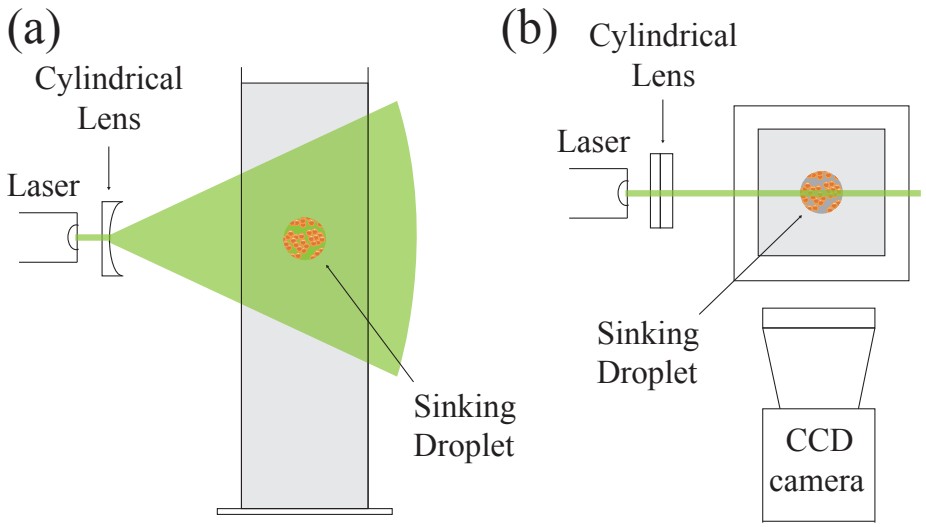

Figure 3: Schematics of the sinking droplet control test. (a) side view (b) top view.

Realizing the functionality of the OpenPIV program, a similar control test was devised to assess the capabilities of the hardware aspects of the system. It consisted of determining the velocity field inside a spherical water droplet as it traveled through a viscous oil medium. Initially, a mixture of water and polystyrene beads with a particle concentration of 10,000 particles per mL of water was prepared. Next, a 30 cm long piece of 10×10 cm square glass tubing was sealed at one end and filled to the top with 1000 cSt silicon oil. The PIV equipment was used such that a laser sheet was aimed through the side of the tubing, with the CCD camera arranged normal to the laser sheet.

Finally, particle filled water droplets, 0.25 mL in volume, were generated at the top of the tubing. Positioned so that the laser sheet sliced through their center, these droplets fell through the tubing while the CCD camera captured an image sequence of the illuminated central plane at 15 frames per second. The schematics of this control test are visually outlined in figure 3, with 3a containing a side view of the experiment and 3b containing a top-down view of the experiment. Eventually the image sequences were processed with OpenPIV and compared to the theoretical expectations.

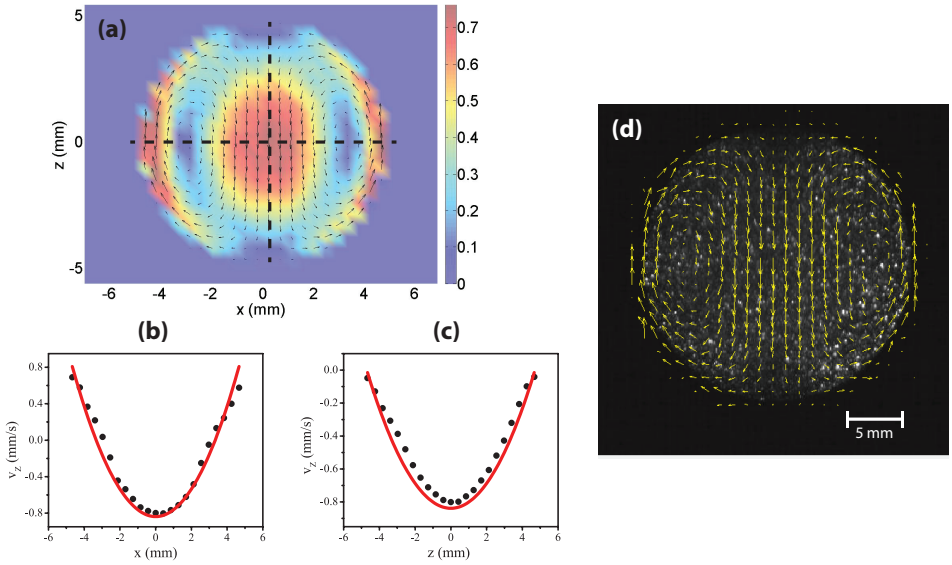

Figure 4: Results of the sinking droplet control test. (a) experimental velocity field (b) horizontal profile (c) vertical profile (d) raw PIV image, scale bar 5 mm.

Figure 4 contains the results of the control test experiment as well as the comparison between experiment and theory. 4a depicts the velocity field produced by OpenPIV with the color indicating the magnitude of the velocity, while 4b and 4c display a comparison between theoretical and experimental velocity across the horizontal and vertical central slices of the droplet, respectively. In both 4b and 4c, the raw data is plotted as black circles, while the theoretical velocity profile is shown as a red curve. 4d contains a single image from the PIV image sequence, with a corresponding velocity field superimposed as yellow arrows. The quality of the results of this test seemed to imply an effective PIV system.

3.3 PIV of Toroidal Droplets

As briefly discussed in the Introduction and Literature Review sections of this thesis, the method used in generating unstable toroidal droplets was that outlined by Pairam and Fernandez-Nieves in ther 2009 publication. Following their specifications, a modified toroidal droplet apparatus was assembled such that PIV could be performed. The apparatus consisted of a freely-rotating metal platform connected to a DC motor. The rotation speed of the motor and platform were controlled by the inclusion of a variably resistor in the motor circuit. Next, a 25×25 mm cuvette was attached to a glass microscope slide such that one end was closed off and the cuvette could stand upright. The modified cuvette was made to attach firmly to the rotating metal platform with neodymium magnets. In order to generate toroidal droplets, the cuvette was filled with $60,000$ cSt silicon oil and rotated. While rotating, a needle was lowered into the cuvette. Subsequently, we injected dispersed phase. The drag between the outer and inner fluid caused formation of a curved jet (figure 5b), which closed on itself (figure 5c), forming a toroidal droplet. A fastening clip attached to a micromanipulator was used to position the needle, and a syringe pump was used to control the volume of fluid within the toroidal droplet. By calibrating needle position and torus volume, the aspect ratio of the toroidal droplets could be systematically varied. In order to capture PIV image sequences of the unstable toroidal droplets as they collapsed, the laser and lens were used to illuminate a cross section of a particle-filled torus as the CCD camera captured images.

As with the sinking-droplet test experiment, the PIV torus experiments were generated with an inner fluid consisting of approximately 10,000 particles per mL. In the experiments to follow, the cuvette was again filled with 60,000 cSt silicon oil, as the high viscosity would lead to slower, more easily-observable collapse. In order to ensure that there was no movement of the free surface during collapse, the toroidal droplets were generated 7 mm from the upper oil-air interface and all edges of the cuvette. This 7 mm distance was determined from a test where silicone oil movement was monitored during toroidal droplet collapse. This was accomplished by taking a top-down video of a toroidal droplet in a silicon oil bath filled with tracer particles and superimposing the first and last frames of the video (figure 6).

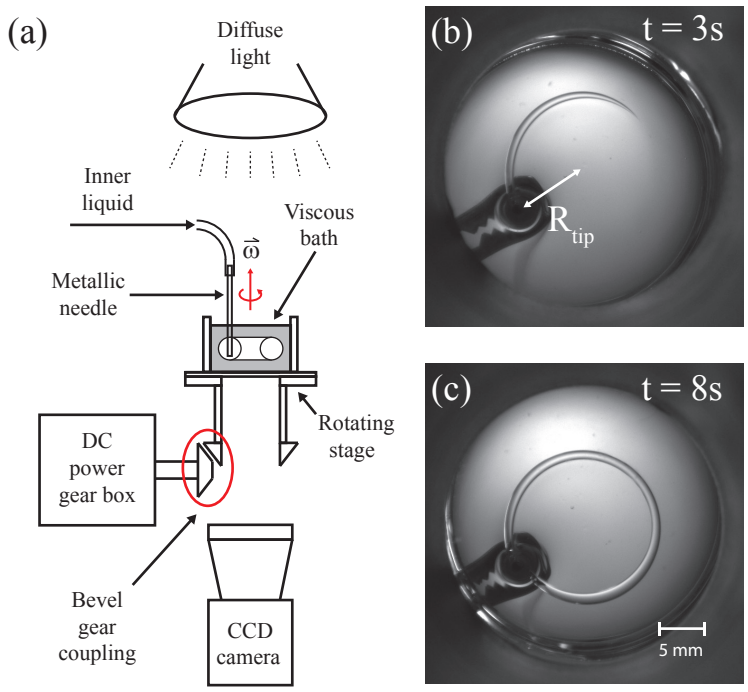

Figure 5: Generation of toroidal droplets in a non-PIV experiment. (a) schematics of the experiment (b) camera image of the toroidal droplet formation at t = 3 seconds (c) camera image of the toroidal droplet formation at t = 8 seconds, scale bar 5 mm.

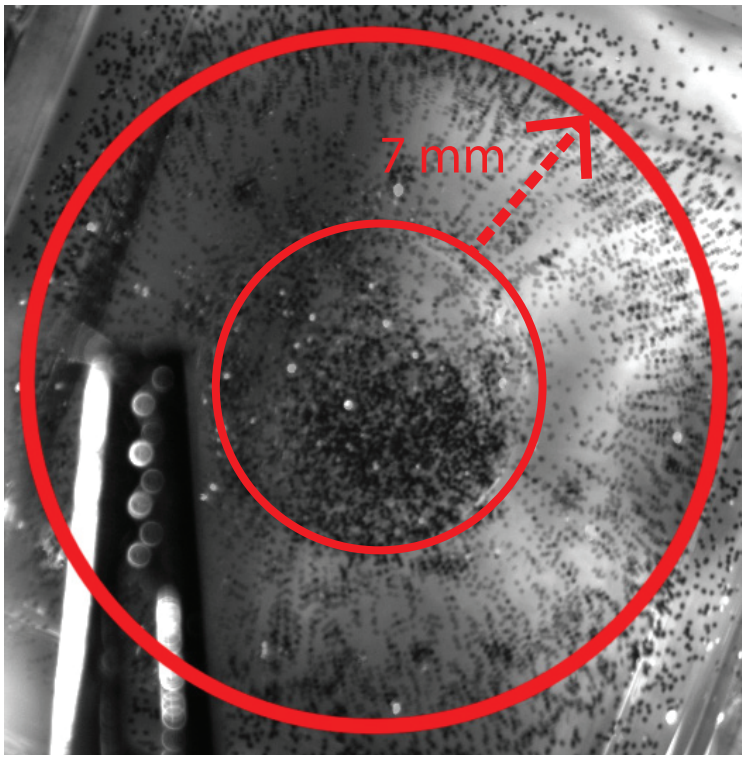

Figure 6: Depth measurement test.

In order to account for any sinking of the torus, it was also necessary to choose an inner fluid that was similar to the silicon oil's density of $0.97\frac{\text{g}}{\text{mL}}$. Furthermore, this inner fluid would have to have a proper interfacial tension with silicon oil such it could form a rounded toroidal droplet that collapsed before particle sedimentation became significant. Ultimately, after testing a series of solutions of varied concentrations of ethanol, water, and glycerol, it became apparent that a 90% glycerol 10% water mixture fit the needs of the experiment. The mixture formed properly shaped toroidal droplets at the required depth, without sinking significantly in the time scale of an experiment, having a density of $1.23\frac{\text{g}}{\text{mL}}$. The Ohnesorge number for the inner fluid was calculated as:

$$Oh \equiv \frac{\eta_i}{\sqrt{\rho a_0 \gamma}} \tag{2}$$

where η_i is the viscosity of the inner liquid, ρ is the density of the inner liquid, γ was the surface tension, and the relevant length scale of the system was chosen to be a_0. Given the properties of the inner liquid, it was determined that $Oh \approx 100 >> 1$, allowing for the Navier-Stokes equation to be

reduced to the Stokes equation in the theoretical calculations contained in the following section.

Having configured a PIV system capable of analyzing unstable toroidal droplets, the system was employed in capturing image sequences of varied toroidal droplets. In each experiment, toroidal droplets of 0.35 mL volume were generated. The position of the needle was varied such that, in keeping volume constant, a wide range of aspect ratios could be observed. Ultimately the velocity-field data that resulted will be compared against the available theoretical flow fields produced from Yao and Bowick's work.

3.4 Theoretical Overview

As mentioned previously, the results from the toroidal droplet PIV experiments will be compared to the only available theoretical work for the velocity field due to Yao and Bowick[10]. This section will attempt to provide a brief overview of their theoretical calculations, regarding the pressure and velocity distributions inside of collapsing toroidal droplets. By taking the divergence of the Stokes equation, while imposing that the fluid is incompressible ($\nabla \cdot \vec{v} = 0$), the pressure distribution can be determined as a solution to the harmonic equation:

$$\Delta p(r, \alpha) = 0 \tag{3}$$

where r and α are defined in figure 1. The harmonic equation reduces to a 2-dimensional problem because of the azimuthal symmetry of the torus. By imposing reflection symmetry across the x-z plane and the fact that the pressure must be finite everywhere, a bipolar coordinate form of the solution may be derived as:

$$p(\zeta, \chi) = \sum_{\nu \in \mathbb{Z}} \alpha_\nu \sqrt{\cosh(\zeta) - \cos(\chi)} Q^0_{\nu - 1/2}(\cosh(\zeta)) \cos(\nu\chi) \tag{4}$$

such that:

$$\cosh \zeta = \frac{R_0}{r} \tag{5}$$

and:

$$\cos\chi = \frac{(R_0/r)\cos\alpha + 1}{(R_0/r) + \cos\alpha} \tag{6}$$

where $Q_\nu^\mu(x)$ is the Associated Legendre functions of the second kind, and α_ν is the coefficient to be determined from the boundary conditions using the Laplace pressure equation:

$$p - p_0 = \gamma H \tag{7}$$

where H is the mean curvature at a point on the surface of the torus:

$$H = \frac{R_0 + 2a_0\cos\alpha}{a_0(R_0 + a_0\cos\alpha)} \tag{8}$$

By expanding the expression for the pressure in equation 4 to the fifth term, the pressure distribution was plotted for the cross-section of a torus' tube, normalized by $\frac{\gamma}{a_0}$ with $p_0 = 1$ in figure 7. In the figure, plots (a) and (b) correspond to toroidal droplets of $\xi = 2.50$ and $\xi = 100$, respectively. The resulting plots show that the pressure is maximized at the outside of the torus ($\alpha = 0$) and minimized at the inside of the torus ($\alpha = \pi$), resulting in the inward shrinkage of the torus. It was also noted that for the $\xi = 100$ toroidal droplet the difference between the maximum and the minimum pressure was significantly lower than that of the $\xi = 2.50$ toroidal droplet. This implies that pressure differential approaches 0 in the thin torus limit as, when local curvature approaches that of a cylinder and $\xi \to \infty$. Hence, the shrinking instability is an inherent feature of toroidal droplets.

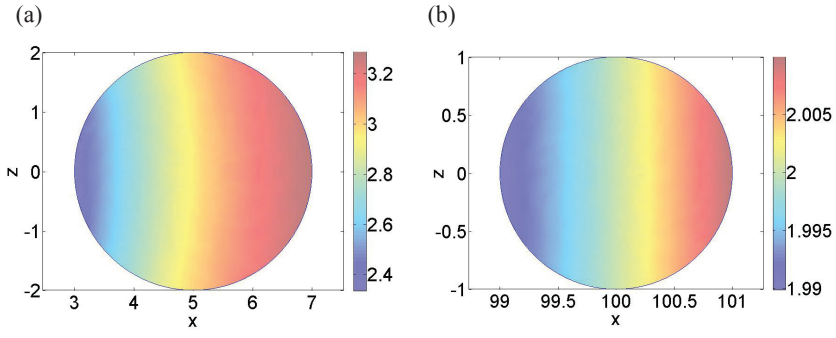

Figure 7: Theoretical pressure distribution within a toroidal droplet. (a) toroidal droplet of $\xi = 2.50$ (b) toroidal droplet of $\xi = 100$.

By treating the fluid as incompressible, the velocity can be written as

$$\vec{v} = \vec{\nabla} \times \vec{\psi} \tag{9}$$

where $\vec{\psi}$ is the vector potential, allowing the curl of the Stokes equation being reduced to the bi-harmonic equation:

$$\Delta^2 \vec{\psi} = 0 \tag{10}$$

Again due to the azimuthal symmetry of the system, all but the θ components of $\vec{\psi}$ disappear, giving rise to a 2-dimensional problem. By imposing the same reflection symmetry across the x-z plane, ψ may be solved as:

$$\psi_\theta(\zeta, \chi) = \frac{d \sinh(\zeta)}{(\cosh(\zeta) - \cos(\chi))^{3/2}} \sum_{\nu \in \mathbb{Z}} C_\nu \sin(\nu\chi) Q^1_{\nu - 3/2}(\cosh(\zeta)) \tag{11}$$

From this, the velocity is obtained by applying equation 9, while the coefficients C_ν are determined by using the no-slip boundary condition. As such, velocity at a point (x_0, z_0) on the interface is calculated as:

$$\vec{v}_{x_0, z_0} = \dot{R}_0 \hat{e}_x + \dot{a}_0 \hat{e}_r \tag{12}$$

where $\dot{R}_0$ is the inward shrinking speed of the toroidal droplet and $\dot{a}_0$ is a tube expansion speed. Yao and Bowick further imposed that the tube's cross-section remains circular, such that:

$$\dot{a}_0 = -\dot{R}_0 \frac{a_0}{2R_0} \tag{13}$$

Figure 8 contains the velocity yields that resulted from the application of the aforementioned theory. Each column in the figure corresponds to a different aspect ratio. From left to right, the aspect ratios are $\xi = 100$, $\xi = 2.50$, $\xi = 1.40$, and $\xi = 1.25$. The first row of the figure is the velocity in the laboratory (stationary) frame, the second row is the velocity in the co-moving frame of the cross-section's centroid, and the third row is a heat-map of the vorticity of the velocity fields in the co-moving frame. This theoretical picture reveals that toroidal droplets shrink for at all values of ξ. Furthermore, at low aspect ratios, the speed distributions tend to reach a maximum

near the interior of the torus and gradually decrease towards the exterior. In the co-moving frame, there is a distinct appearance of a source, the location of which varies with respect to aspect ratio. This source indicates growth in the cross-section, which is reasonable considering that volume is conserved. Regarding the vorticity, in all cases the sign of the vorticity indicates that the circulation is counter clockwise for $z > 0$ and clockwise for $z < 0$.

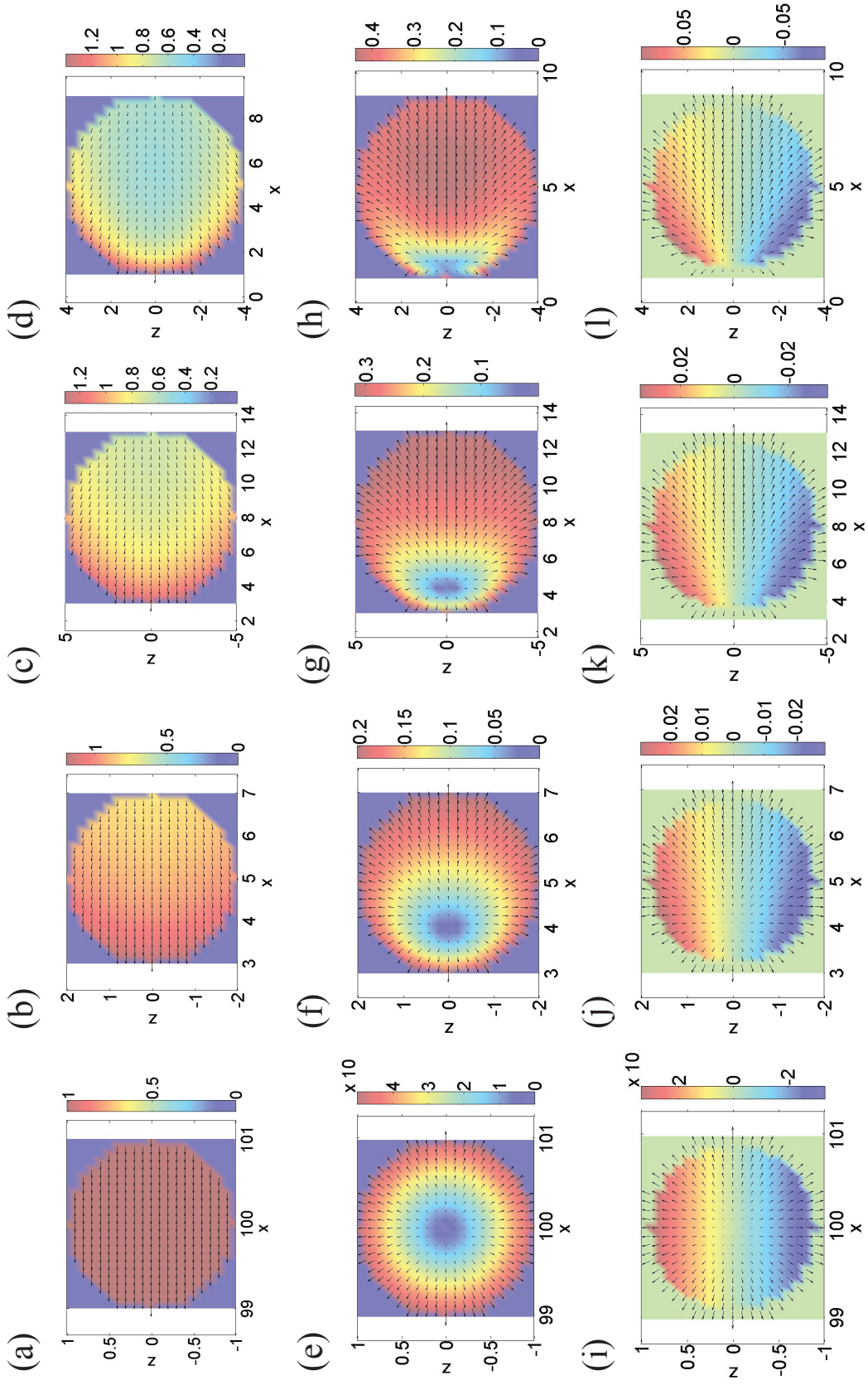

Figure 8: Theoretical velocity fields for toroidal droplets of various aspect ratios. (a,e,i) $\xi = 100$ (b,f,j) $\xi = 2.50$ (c,g,k) $\xi = 1.40$ (d,h,l) $\xi = 1.25$. First row of images: velocity in laboratory frame. Second row of images: velocity in the droplet centroid frame. Third row of images: vorticity in the droplet centroid frame.

CHAPTER IV

RESEARCH RESULTS

Figure 9 contains a typical result obtained from a successful PIV experiment for a collapsing toroidal droplet. In the figure, the yellow arrows correspond to the velocity field generated by the PIV analysis software and are superimposed on the corresponding image from the PIV image sequence. Note that the clarity of the vector field on the right portion of the toroidal droplet appears to be of higher quality then that of the left portion of the droplet. It was ultimately concluded that this improved clarity was a result of the fact that the laser light shone in from the right. As such, all further data analysis was performed solely on the right portions of the PIV data, which was allowed by argument of azimuthal symmetry.

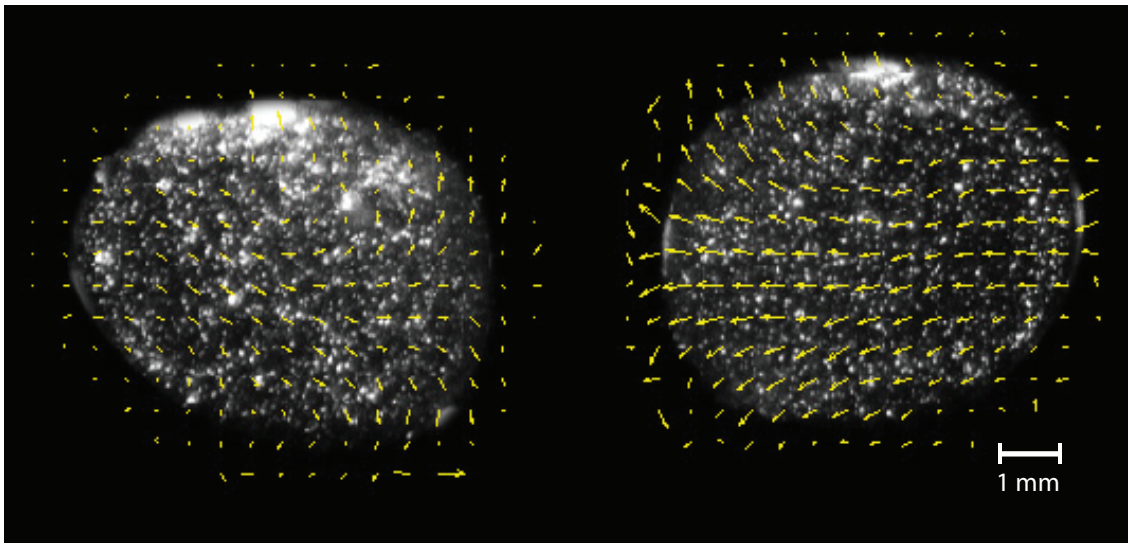

Figure 9: PIV vector field superimposed on the corresponding image, scale bar 1 mm.

Figure 10 contains a qualitative visualization of the manner by which the cross-section of a toroidal droplet evolves throughout the duration of a collapsing experiment. Note that at the beginning of the experiment, the cross section is almost elliptical, but at $t = 5$ seconds the cross section deviates substantially from its initial shape. This trend was observed for all aspect ratios.

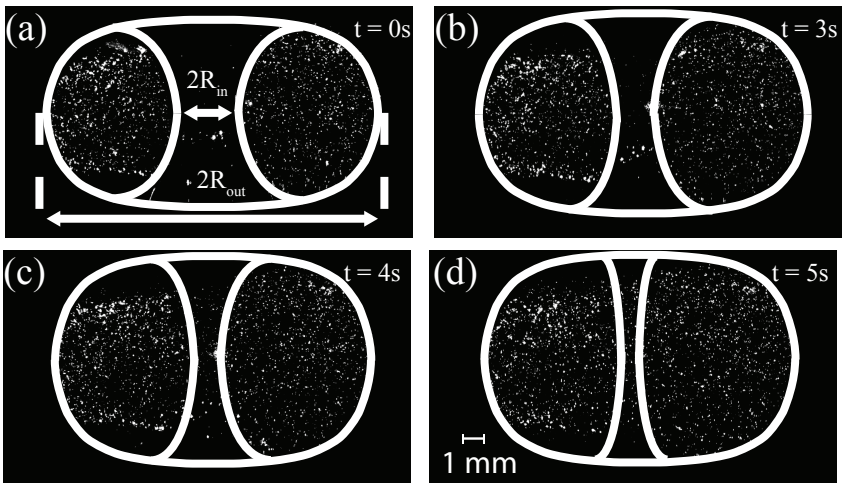

Figure 10: Visualization of the geometrical evolution of the toroidal droplet. (a) t = 0 seconds (b) t = 3 seconds (c) t = 4 seconds (d) t = 5 seconds, scale bar 1 mm.

Figure 11 contains the data that resulted from the analysis of several collapsing toroidal droplets of varied aspect ratio. The first row of images in the figure (a-d) contain the resulting velocity fields as observed in the laboratory frame, the second row of images (e-h) contains the same velocity fields as observed in the co-moving frame of the centroid of the cross section, and the third row of images (i-l) contains the vorticities corresponding to the velocity fields in the co-moving frame. Each column of the figure corresponds to the results of the PIV analysis of an individual toroidal droplet. Observed from left to right, the aspect ratios of the toroidal droplets are $\xi = 1.6$, $\xi = 1.3$, $\xi = 1.2$, and $\xi = 1.1$, respectively. On a qualitative level, it was noted that all of the experiments showed similar velocity distributions when observed in the laboratory frame. In all cases, the maximum velocity was located towards the inner part of the toroidal droplet, and gradually decreased towards the outer part of the droplet. The vorticity maps also showed a certain degree of consistency across all of the toroidal droplets, having positive vorticity in the lower left portion of the droplet and negative vorticity in the upper left portion of the droplet. In the co-moving frame, the velocity fields had similarities, but the location of the source appeared to move towards the right part of the toroidal droplet as aspect ratio decreased.

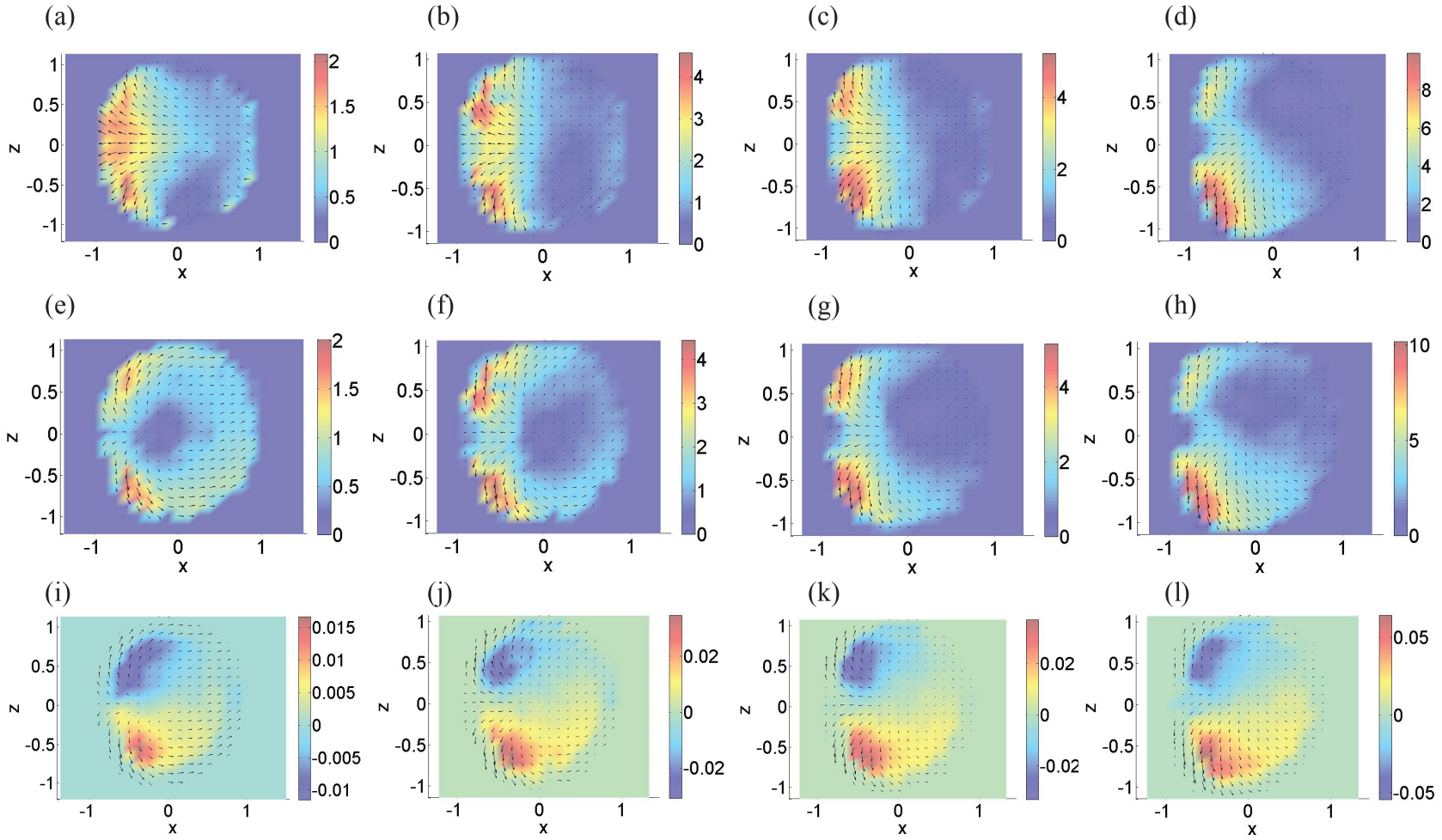

Figure 11: Vector fields that resulted from the PIV analysis of toroidal droplets of varied aspect ratios. (a,e,i) $\xi = 1.6$ (b,f,j) $\xi = 1.3$ (c,g,k) $\xi = 1.2$ (d,h,l) $\xi = 1.1$. First row of images: velocity in laboratory frame. Second row of images: velocity in the droplet centroid frame. Third row of images: vorticity in the droplet centroid frame.

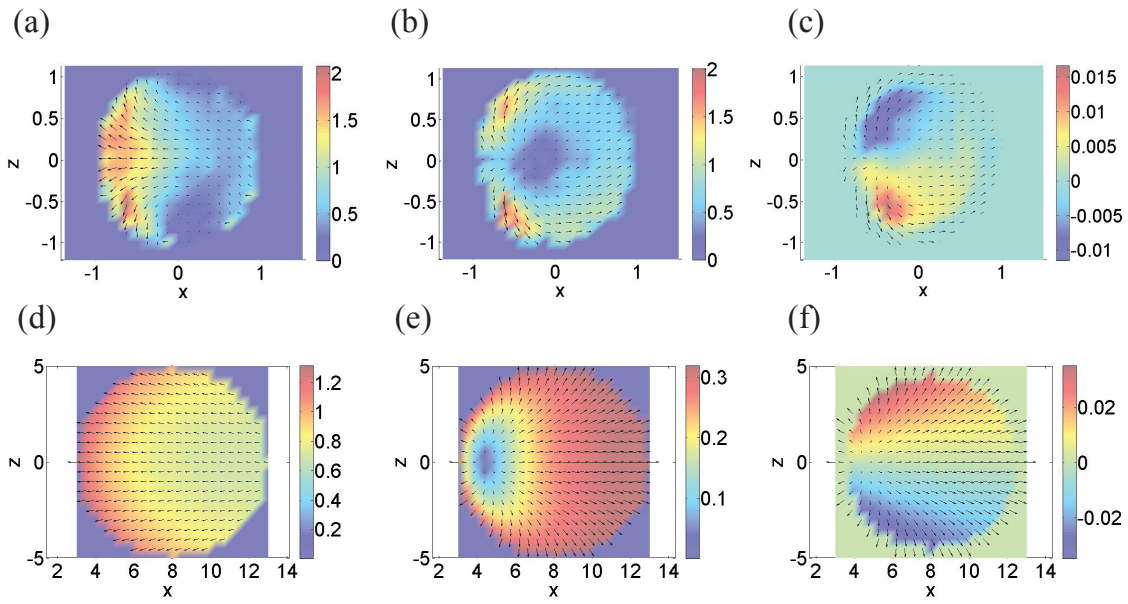

Figure 12: Comparison of the experimental vector fields to the theoretical vector fields for a toroidal droplet of $\xi = 1.6$. (a,d) velocity in the laboratory frame (b,e) velocity in the droplet centroid frame (c,f) vorticity in the droplet centroid frame. First row of images: experimental vector fields. Second row of images: theoretical vector fields.

Figure 12 contains a comparison of the experimentally obtained PIV vector fields (a-c) to the corresponding theoretical vector fields (d-f) predicted by the model suggested by Yao and Bowick. Both the experimental and theoretical vector fields correspond to a toroidal droplet of aspect ratio, $\xi = 1.6$. From left to right, the columns of the figure contain the velocity field in the laboratory frame, the velocity field in the co-moving frame, and the vorticity map of the velocity field in the co-moving frame. Though the experimental velocity fields reveal similar velocity distributions, and the presence of a source, there appears to be an appreciable disagreement between experiment and theory. Regarding the vorticity fields, the experimental field showed a similar division between the top and bottom half of the droplet, though the direction of the vorticities were reversed for the theoretical expectations.

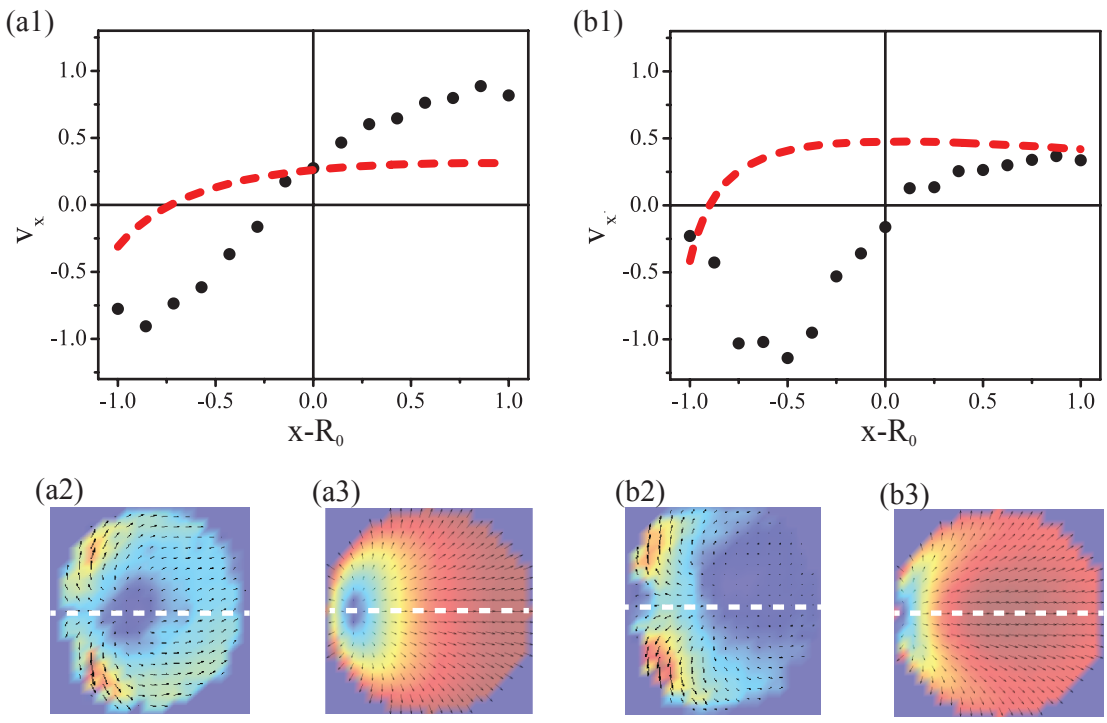

Figure 13: Additional comparison of theoretical and experimental velocity fields. (a1) the cross-section velocity comparison for a $\xi = 1.6$ toroidal droplet (b1) the cross-section velocity comparison for a $\xi = 1.2$ toroidal droplet. (a2,a3) the experimental and theoretical velocity fields corresponding to the data plotted in (a1), respectively. (b2,b3) the experimental and theoretical velocity fields corresponding to the data plotted in (b1), respectively.

Figure 13 contains the results of a further comparison between the theoretical predictions and the experimental results. The two graphs at the top of the figure, a1 and b1, contain plots of the x-components along the horizontal lines through the center of the droplet shown in the velocity field images below. The red dashed lines in the plots correspond to the theoretically predicted values, while the black correspond to the experimental data. Plots (a1), (a2), and (a3), correspond to a droplet of $\xi = 1.6$, while plots (b1), (b2), and (b3) correspond to a droplet of $\xi = 1.2$. As can be seen, there is important disagreement between theory and experiment.

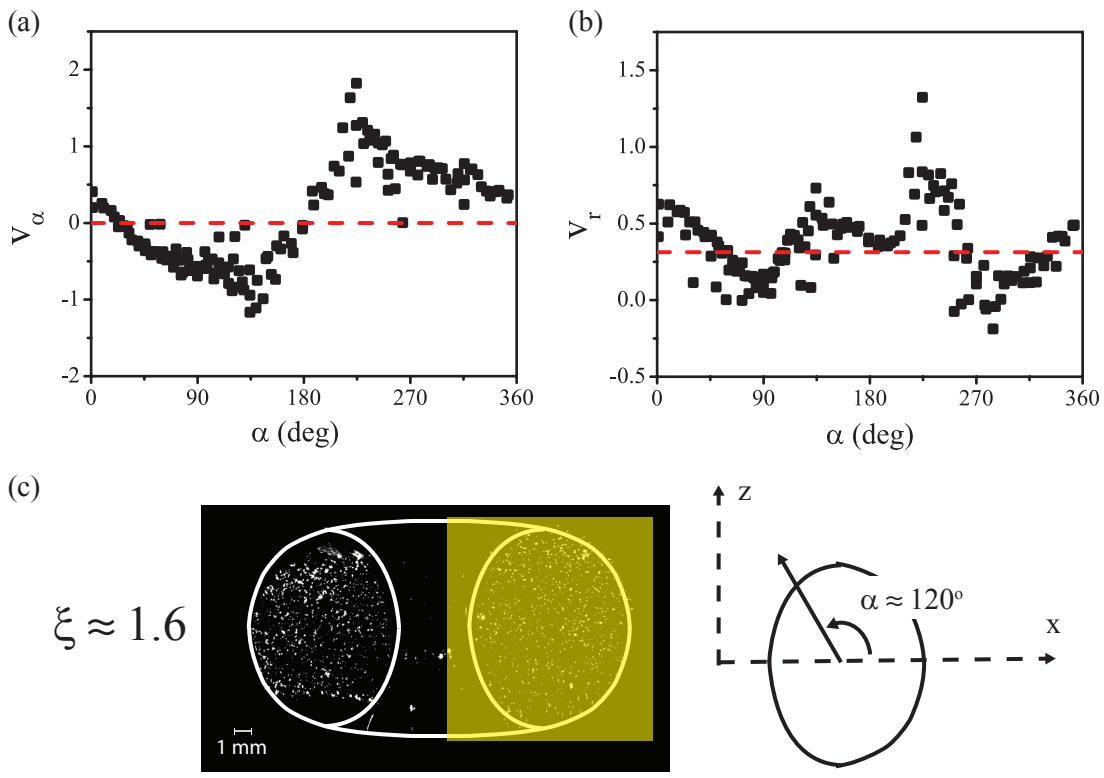

Figure 14: Boundary velocity comparison. (a) the angular component of the boundary velocity (b) the radial component of the boundary velocity (c) the manner by which the plots proceed, scale bar 1 mm.

The final analysis used in comparing the PIV analysis results to the theoretical velocity fields involved a measurement of the velocities at the boundaries of the droplet. The results of the measurement are contained in figure 14. In the figure, (a) contains a plot of tangential velocity as a function of angular displacement with the theory plotted as a red dashed line and the experimental data plotted as black points. A similar plot for the radial velocity as a function of angular displacement is displayed in (b). Angular displacement was measured in the manner depicted in (c). Tangential and radial velocities were measured by approximating the cross section of the toroidal droplets with an ellipse. Based on the analysis, a distinct difference persisted between experiment and theory. The theory predicted constant angular and radial velocities, while the experiments showed significant variation with respect to angular displacement.

CHAPTER V

DISCUSSION AND CONCLUSION

Upon completion of the PIV experiments discussed in the preceding chapters, it is clear that the proposed methods allowed for the successful capture of PIV image sequences of collapsing toroidal droplets in a controlled manner. Furthermore, on a qualitative level, the results of the experiments agreed with the majority of the theoretically suggested predictions. In each of the experiments the co-moving frame velocity fields revealed the presence of a source, the location of which varied with respect to aspect ratio in a similar manner to the theory. The existence of sources was indicative of the cross-sectional growth predicted by the most basic principles of volume conservation. In addition to the presence of the sources, there were also similarities between the velocity fields in the stationary frame. In theory and experiment, the velocity was highest towards the innermost part of the toroidal droplet and decreased towards the outermost part. In both theory and experiment, vorticity achieves a minimum at $z = 0$.

The PIV experiments also served to shine some light on the geometrical evolution of collapsing toroidal droplets. In all of the experiments, the cross sections of the droplets appreciably differed from circular as they underwent collapse.

When observed through a more quantitative lens, the experimental results differ substantially from the theoretical picture. As shown in the horizontal profile comparisons, the experimental data exhibits a prominent minimum in x-velocity towards the inner part of of the droplet. The same minimum is absent in the theoretical velocity fields. To the right of the minimum, the experimental data contains similar curvature to the theoretical data. This may have been a result of the boundary conditions imposed by the theory.

The results of the boundary velocity comparison also revealed a staunch difference between the experimental results and the theory. Though not reminiscent of a well-known function, the experimental data revealed the presence of extrema for both the radial and tangential boundary velocities,

when plotted as a function of angular displacement. In contrast, the theoretically predicted tangential velocity is zero along the entire boundary. The radial velocity was predicted to be a constant positive value due to the assumed circular cross-section of the droplet during the collapsing process. As such, the experimental results seem to imply that the imposed boundary conditions fail to capture the reality of the system. If the observations from these experiments are accounted for in the theoretical model, it is not unreasonable to expect that the theory will capture the data more accurately.

CHAPTER VI

FUTURE WORK

Though the results of the experiments outlined in this thesis point in a promising direction, there is ultimately still much work do be done before any concrete conclusions can be achieved. Primarily, it's essential that more data be obtained across the board, both for toroidal droplets of the aspect ratios already captured and at additional aspect ratios. Though the current technique for generating PIV image sequences was sufficient for a preliminary study, it encounters difficulty when exploring toroidal droplets of larger aspect ratios. As such, a refinement of the technique is also necessary for the eventual continuation of this exploration. In addition to analyzing a larger pool of toroidal droplet videos, it would also be interesting to explore the velocity field of the outer fluid as toroidal droplets collapse. Such an analysis could provide additional insight regarding the exact nature of the boundary conditions and contribute to a more complete picture of the system.

In addition to the aforementioned experimental expansions, it is also essential that the theory be modified to capture the experimental observations. Even at the present state, the experimental data seems to imply that the theoretical picture of collapsing toroidal droplets fails to capture the full story. If the theory is refined such that it incorporates cross-sectional shape evolution and the new boundary conditions, it would provide for further scrutiny of the experimental data and help bridge the gap between the mathematical and physical explanations of the system.

REFERENCES

[1] Boys, C., *Soap Bubbles - Their Colours and the Forces Which Mould Them*. New York: Dover, 1959.

[2] Earle, R., "Unit operations in food processing." http://www.nzifst.org.nz/unitoperations/sizereduction2.htm. Accessed: 2015-04-9.

[3] Hill, R. and Eaves, L., "Nonaxisymmetric shapes of a magnetically levitated and spinning water droplet," *Physical Review Letters*, vol. 101, Dec. 2008.

[4] Mehrabian, H. and Feng, J. J., "Capillary breakup of a liquid torus," *J. Fluid Mech.*, vol. 717, pp. 281–292, 2013.

[5] Pairam, E. and Fernandez-Nieves, A., "Generation and stability of toroidal droplets in a viscous liquid," *Physical Review Letters*, vol. 102, June 2009.

[6] Plateau, J. *Acad. Sci. Bruxelles Mem.*, vol. 23, no. 5, 1849.

[7] Plateau, J., "Experimental and theoretical statics of liquids subject to molecular forces only," *Dr. Dobb's Journal*, vol. 1, 1873.

[8] Rayleigh, L. *Proc. Row. Soc. Londonl*, vol. 29, no. 71, 1879.

[9] Walters, J. and Davidson, J., "Literate programming," *J. Fluid Mech*, vol. 17, pp. 321–336, May 1963.

[10] Yao, Z. and Bowick, M. J., "The shrinking instability of toroidal liquid droplets in the stokes flow regime," *Eur. Phys. J.*, vol. 34, Mar. 2011.

VITA

Eric M. Berger was born in an insignificant town on an insignificant day.